AMERICAN JOURNAL OF INNOVATION IN SCIENCE AND ENGINEERING (AJISE)

ISSN: 2158-7205 (ONLINE)

VOLUME 3 ISSUE 2 (2024

PUBLISHED BY
E-PALLI PUBLISHERS, DELAWARE, USA

American Journal of Innovation in Science and Engineering (AJISE)

Volume 3 Issue 2, Year 2024
ISSN: 2158-7205 (Online)
DOI: https://doi.org/10.54536/ajise.v3i2.2774
https://journals.e-palli.com/home/index.php/ajise

Study of the Sources of Instability Observed at the Outlet of the Lagdo Dam Penstock

Tchawe Tchawe Moukam[1*], Tientcheu Nsiewe Max-Well[2], Djiako Thomas[3], Tcheukam Toko Dénis[4], Kenmeugne Bienvenu[5]

Article Information

Received: June 19, 2024
Accepted: July 23, 2024
Published: July 26, 2024

Keywords

Instability Source, Penstock, Hydroelectric Plant, CFD

ABSTRACT

The Lagdo hydropower plant is the smallest of three plants designed before the 1990s in Cameroon. It has a capacity of 72 MW and is the main source of energy for the North Interconnected Network (NIN). This facility has been experiencing several problems over the past ten years and is increasingly unsatisfactory in terms of service. This is due to several parameters, including the instability observed in the flow structure. In this paper, we have evaluated some parameters that may be at the origin of these instabilities by a numerical approach, followed by field observations. It appears from this study that in addition to the dynamic field variation parameter (pressure and velocity) involved in the creation and propagation of instabilities, others, such as the water level in the upstream reservoir and the variation of the turbulent friction, are also to be considered.

INTRODUCTION

Globally, renewable energies now account for 19.3% of final electricity consumption in 2017, compared to 78.4% for fossil fuels and only 2.3% for nuclear (Global Architecture Performance Index Report – WEF, 2017). As for the African continent, many countries produce their electricity from renewable sources, led by Ethiopia, which is at around 93.9%. Cameroon ranks 16th on the continent with about 70% of its energy production (Global Architecture Performance Index Report – WEF, 2017).

The Lagdo hydropower plant is the smallest of the three oldest hydropower plants in the country, with a capacity of 72 MW (Bikidik, 2014). Its position in a low slope area makes it particularly vulnerable, as it is more exposed to certain hydraulic phenomena (water hammer, cavitation, etc.). Located in the northern part of the country, the rainy season covers a shorter period than the dry season. Thus, the variation of the approach water height during these two year periods is considerable. Thus, in this work it will be investigated the impact of each of these elements on the flow structure. Similarly, other factors such as the nature of the soil and the shape/position of the water intake will be observed on this instability phenomenon.

MATERIALS AND METHODS

Materials

With a Latitude 9° 3'35.43"N, a longitude 13°41'21.81"E, and located 50 km south of Garoua in the middle of the Sahelian zone, is the Lagdo hydroelectric dam that was built in the years 1978-1984 by Cameroonians with the help of Chinese engineers and workers. A view of the downstream tank is shown in figure 1 below.

Figure 1: Lagdo dam (Energy of Cameroon (ENEO S.A.)

The Benue, in its Chadian- Cameroonian course, drains a catchment area of 97,000 km², of which 60,000 km² is south of the Garoua parallel; the rest is in the North and East. Its total length, from the source to the confluence with the Faro, is 350 km of which 220 km are upstream of the dam and 130 downstream (Tchotsoua, 2007).

According to Ngatcha *et al.* (2002), the reservoir upstream of this dam has a potential of 7.7 billion m3. The flooded area at elevation 216m (normal level of the reservoir) is 697 km². The Benue River has its source at an altitude of 1,300 m on the Adamaoua plateau. It is the main tributary of the Niger River and the major collector of the Lower Niger in terms of inflows. The highest average flows are observed in September, while April is the month of lowest water levels. The maximum flood occurred in September when in 1966 it reached 3428 m³/s. In Garoua, the maximum observed flood flow was 6,130 m³/s on 26 August 1948, the daily flow corresponding to this flood was 5970 m³/s. The Benue is a river with an essentially

[1] Department of Mechanical Engineering, ENSAI, University of Ngaoundere, Cameroon
[2] Department of Fundamental Sciences, EGCIM, University of Ngaoundere, Cameroon
[3] Department of Mechanical Engineering and Energy, ISTA, University Institute of the Gulf of Guinea, Cameroon
[4] Department of Mechanical Engineering, COT, University of Buea, Cameroon
[5] Department of Mechanical Engineering, ENSPY, University of Yaounde 1, Cameroon
[*] Corresponding author's e-mail: christophetchawe88@gmail.com

sandy bed that experiences variations during major floods

METHODOLOGY

In order to carry out this work, we used the Fluent software, which has a large number of turbulence models to deal with many physical problems. The geometry of the structure was modelled in Gambit 2.2, as well as the definition of the types of boundary conditions in the physical domain and the specification of the parameters characterizing the fluid-structure interaction. For the pressure-velocity coupling, the SIMPLEC algorithm was adopted and the discretization scheme used the Power Low.

For an incompressible fluid where the viscosity is constant, the motion can be described using second order partial differential equations of the following form (Tchawe *et al.*, 2018):

$\partial u/\partial x+\partial v/\partial y+\partial w/\partial z = 0$ (1)

The dimensionless spatial and hydrodynamic variables characterizing this flow will then be (Tchawe *et al.*., 2018):

Table 1: Summary of dimensionless spatial and hydrodynamic variables

$\bar{x}=x/L$	$\bar{y}=y/L$	$\bar{z}=z/H$	$\bar{u}=u/U_\infty$	$\bar{v}=v/U_\infty$	$\bar{w}=w/U_\infty$	$\bar{p}=(p-p_\infty)/(\varrho U^2_\infty)$

The previous Navier-Stockes system (1) is thus put into the following dimensionless form:

$$\begin{cases} \bar{u}\dfrac{\overline{\partial u}}{\partial x}+\bar{v}\dfrac{\overline{\partial v}}{\partial y}+\bar{w}\dfrac{\overline{\partial w}}{\partial z}=-\dfrac{\overline{\partial p}}{\partial x}+\dfrac{1}{Re}\left(\dfrac{\overline{\partial^2 u}}{\partial x^2}+\dfrac{\overline{\partial^2 v}}{\partial y^2}+\dfrac{\overline{\partial^2 w}}{\partial z^2}\right) \\ \bar{u}\dfrac{\overline{\partial u}}{\partial x}+\bar{v}\dfrac{\overline{\partial v}}{\partial y}+\bar{w}\dfrac{\overline{\partial w}}{\partial z}=-\dfrac{\overline{\partial p}}{\partial y}+\dfrac{1}{Re}\left(\dfrac{\overline{\partial^2 u}}{\partial x^2}+\dfrac{\overline{\partial^2 v}}{\partial y^2}+\dfrac{\overline{\partial^2 w}}{\partial z^2}\right) \\ \bar{u}\dfrac{\overline{\partial u}}{\partial x}+\bar{v}\dfrac{\overline{\partial v}}{\partial y}+\bar{w}\dfrac{\overline{\partial w}}{\partial z}=-\dfrac{\overline{\partial p}}{\partial z}+\dfrac{1}{Re}\left(\dfrac{\overline{\partial^2 u}}{\partial x^2}+\dfrac{\overline{\partial^2 v}}{\partial y^2}+\dfrac{\overline{\partial^2 w}}{\partial z^2}\right) \end{cases} \quad (3)$$

with $Re= (UD_h)/(\vartheta)$ being the determining parameter for the scaling effect.

The energy equation is therefore represented by the relationship below (Tcheukam-Toko *et al.*., (2012):

$\partial T/\partial t+u\ \partial T/\partial x+v\ \partial T/\partial y+w\ \partial T/\partial z = a((\partial^2 T)/(\partial x^2)+(\partial^2 T)/(\partial y^2)+(\partial^2 T)/(\partial z^2))$ (4)

The transformation of the momentum equation into an equation linking dimensionless quantities makes it possible to highlight some of the dimensionless parameters. We therefore define a list of physical reference quantities for our case by:

- Dimensionless coordinates x: $x^*= x/L$; $x^+= r/D$;
- Dimensionless coordinates y: $y^*= y/L$; $y^+= r/D$;
- Scaled coordinates z: $z^*= z/H=z/H_\infty$; $z^+= r/D$;
- Dimensioned velocity U: $u^*= u/U_\infty$; $u^+= v^2/U^2$;
- Dimensioned velocity V: $v^*= v/U_\infty$; $v^+= v^2/U^2$;
- Dimensioned velocity W: $w^*= w/U_\infty$; $w^+= v^2/U^2$;
- Dimensioned pressure p: $p^*= p/P_\infty$;
- Dimensioned viscosity: $\mu^*=\mu/\mu_\infty$.

These results will also depend on the parameters defined by the following relationships:

The Reynolds number Re which is the determining parameter for the scaling effect. It physically represents the ratio of the inertial forces and the viscous forces exerted on a fluid particle, i.e.:

$Re= (UD_h)/(\vartheta)$ (5)

In fact, the Reynolds analogy introduces similarity in the boundary layers where viscous forces and other more complex phenomena such as disbonds occur. In a way, it ensures that the forces measured on a model can be extrapolated to the real structure;

$(\partial u)\overline{\ }/(\partial x)\overline{\ }+(\partial v)\overline{\ }/(\partial y)\overline{\ }+(\partial w)\overline{\ }/(\partial z)\overline{\ }=0$ (2)

Hence:

✤ The turbulence intensity I, given in percentage, which is the ratio between the velocity fluctuations and its average:

$$I=\sqrt{\frac{\overline{u'^2}}{U^2}}=\frac{u'}{U} \quad (6)$$

where u and u' are the moduli of the velocity and its fluctuation respectively. As this information is not sufficient to define the turbulent character of the flow, Fluent uses an implicit approximation to determine the turbulent viscosity μt. The table below summarizes the associations made automatically by the software:

Table 2: Turbulent intensity and associated viscosity (Olivier, 2013)

I	μ_t/μ
0,01	1
0,05	10
0,10	100

In this case, both pieces of information are used to first calculate k using the specified intensity:

$k = 3/2\ I^2\ U^2$ (7)

and then ε from the implicitly determined viscosity ratio:

$\varepsilon = \varrho C\mu\ k^2/\mu_t$ (8)

Alternatively, another option giving more control to the user is to use I but specify a length scale characteristic of turbulent fluctuations, Le. This length is then used instead of μt to determine the dissipation rate ε, once k, using the expression:

$\varepsilon= k^{(3/2)}/L_e$ (9)

The turbulence intensities for the velocity components v and w are defined in the same way.

Pressure coefficient: the action of the pressure is carried out according to Cauchy's principle according to the normal to the wall and proportionally to the static pressure p. The elementary pressure force dF exerted on a surface element dS of unit normal vector N is written simply:

$C_p = (P-P_{ref})/(1/2\ \varrho\ U^2_{ref})$ (10)

This parameter is relatively independent of the flow velocity and is only related to the geometry of the structure. However, it can depend on the Reynolds number due to variations in the position of the boundary layer separation and re-bonding points on non-profiled structures (case of a circular cylinder). We adopted the following decomposition for pressure and velocity:

$$\underline{u} = \overline{\underline{u}} + \underline{u'} \quad (11)$$

$$p = \overline{p} + p' \quad (12)$$

The decomposition of the viscous stress tensor is written:

$$\underline{\underline{\tau}} = \overline{\underline{\underline{\tau}}} + \underline{\underline{\tau'}} \quad (13)$$

with the viscous stress tensor given by:

$$\begin{cases} \overline{\tau_{ij}} = \mu\left(\frac{\partial \overline{u_i}}{\partial x_j} + \frac{\partial \overline{u_j}}{\partial x_i}\right) - \frac{2}{3}\mu\frac{\partial \overline{u_k}}{\partial x_k}\delta_{ij} \\ \vdots \\ \tau'_{ij} = \mu\left(\frac{\partial u'_i}{\partial x_j} + \frac{\partial u'_j}{\partial x_i}\right) - \frac{2}{3}\mu\frac{\partial u'_k}{\partial x_k}\delta_{ij} \end{cases} \quad (14)$$

For the Reynolds tensor closure problem, Boussinesq (1877) also proposed a model closure equation in the form:

$$-\rho\overline{u'_i u'_j} = \mu_t\left(\frac{\partial u_i}{\partial x_j} + \frac{\partial u_j}{\partial x_i}\right) - \frac{2}{3}\left(\rho k + \frac{\partial u_i}{\partial x_j}\right)\delta_{ij} \quad (15)$$

The modelling of turbulence in this framework is to have a relationship between μ and the other unknowns of the problem in order to close the system of equations to be solved. The k-ε turbulence model adds two additional transport equations to the system in addition to the continuity equation and the three RANS equations. A proportionality coefficient is introduced which is obtained experimentally (Prandtl, 1925):

$L_t = c_\mu\ k^{(3/2)}/\varepsilon$ (16)

With these two variables, the turbulent viscosity μt can be calculated:

$u_t = \varrho c_\mu\ k^2/\varepsilon$ or $v_t = c_\mu\ k^2/\varepsilon$ (17)

The two variables k and ε must be calculated to determine v_t as stated above. The equations of the turbulent kinetic energy and its dissipation rate give us:

$$\begin{cases} \rho\overline{u_j}\frac{\partial \varepsilon}{\partial x_j} = \frac{\mu_i}{\sigma_k}\frac{\partial^2 k}{\partial {x^2}_j} + \rho p_k - \rho\varepsilon \\ \rho\overline{u_j}\frac{\partial \varepsilon}{\partial x_j} = \frac{\mu_i}{\sigma_\varepsilon}\frac{\partial^2 \varepsilon}{\partial {x^2}_j} + \rho\frac{\varepsilon}{k}(c_{\varepsilon 1}p_k) - c_{\varepsilon 2}\varepsilon \end{cases} \quad (18)$$

These equations can be rewritten for the turbulent kinetic energy as:

$$\overline{u_j}\frac{\partial k}{\partial x_j} = c_\mu\frac{k^2}{\varepsilon}\left(\frac{\partial \overline{u_i}}{\partial x_j} + \frac{\partial \overline{u_j}}{\partial x_i}\right)\frac{\partial \overline{u_i}}{\partial x_j} + \frac{\partial}{\partial x_j}\left(\frac{c_\mu k^2}{\sigma_k \varepsilon}\frac{\partial k}{\partial x_j}\right) - \varepsilon \quad (19)$$

The term on the left represents the change in turbulent kinetic energy. On the right, the first term represents the generation of turbulent kinetic energy; the second term represents diffusion; and the last term represents dissipation. The dissipation energy equation is given by the equation:

$$\overline{u_j}\frac{\partial \varepsilon}{\partial x_j} = c_{\varepsilon 1}c_\mu k\left(\frac{\partial \overline{u_i}}{\partial x_j} + \frac{\partial \overline{u_j}}{\partial x_i}\right)\frac{\partial \overline{u_i}}{\partial x_j} + \frac{\partial}{\partial x_j}\left(\frac{c_\mu k^2}{\sigma_\varepsilon \varepsilon}\frac{\partial \varepsilon}{\partial x_j}\right) - c_{\varepsilon 2}\frac{\varepsilon^2}{k} \quad (20)$$

The constants determined from the elementary experiments are:

$c_\mu = 0.09$ $\sigma_k = 1.3$ $c_{\varepsilon 1} = 1.44$ $c_{\varepsilon 2} = 1.92$ (21)

In order to adopt the appropriate mathematical formulation, it is essential to highlight the input parameters governing our study in its various configurations; hence, the following simplifying assumptions for the study carried out:

- ➢ The incoming flow is stationary;
- ➢ The fluid is incompressible;
- ➢ Turbulence is isotropic: Reynolds number is high enough (18.6×10^6 <Re <23.16×10^6) so that the anisotropy character is not taken into account;
- ➢ Air resistance is negligible.

RESULTS AND DISCUSSION

Modelling of the structure and boundary conditions

The study area is that between the intake dam (20m upstream of the intake), and the penstock outlet (spiral tank inlet) as modelled in Figure 2 below.

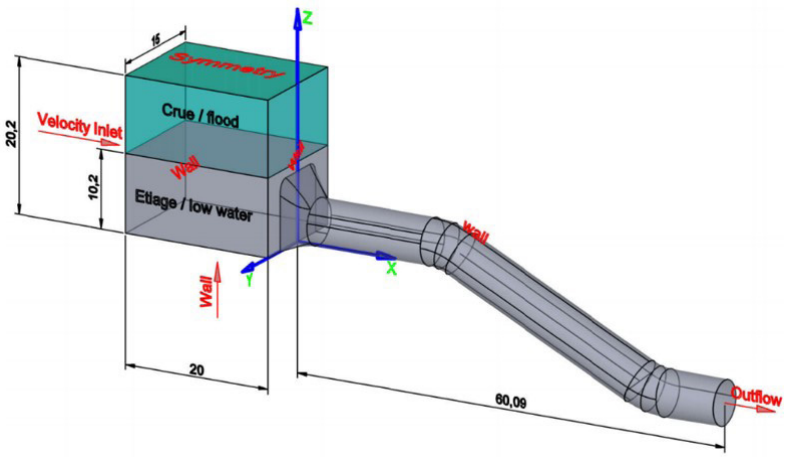

Figure 2: Lagdo Dam modelled in Gambit 2.2.

As inlet flow parameters and basic information about the penstock, we have the following data:

- ➢ The observed minimum flow rate, Q = 109 m^3/s;
- ➢ The diameter of the pipe, Dc = 6 m;
- ➢ The length of the pipe ≈ 65 m.

The Lagdo dam has an average interannual operation of 4470 hours. The average annual productivity is 291 Gwh/year. The velocity conditions at the walls and openings are presented on the figure 2.

Investigation of Potential Sources of Instability

After obtaining the field data and the results of the numerical simulation, a number of sources were identified. Subsequently, we will present four (04) factors that can be summarized in three (03) parameters: the dynamic field parameter, the season parameter and the shape parameter of the structure.

Velocity-Related Factors

This factor is the first element of the dynamic field parameter. The objective is to highlight the impact of the flow velocity on the structure of the fluid layers. For this purpose, three Reynolds numbers corresponding to three annual flow rates will be considered. Emphasis will be placed on the flow in the elbows and at the outlet of the penstock, with two sections, each on both sides of the elbow and a single section for the outlet.

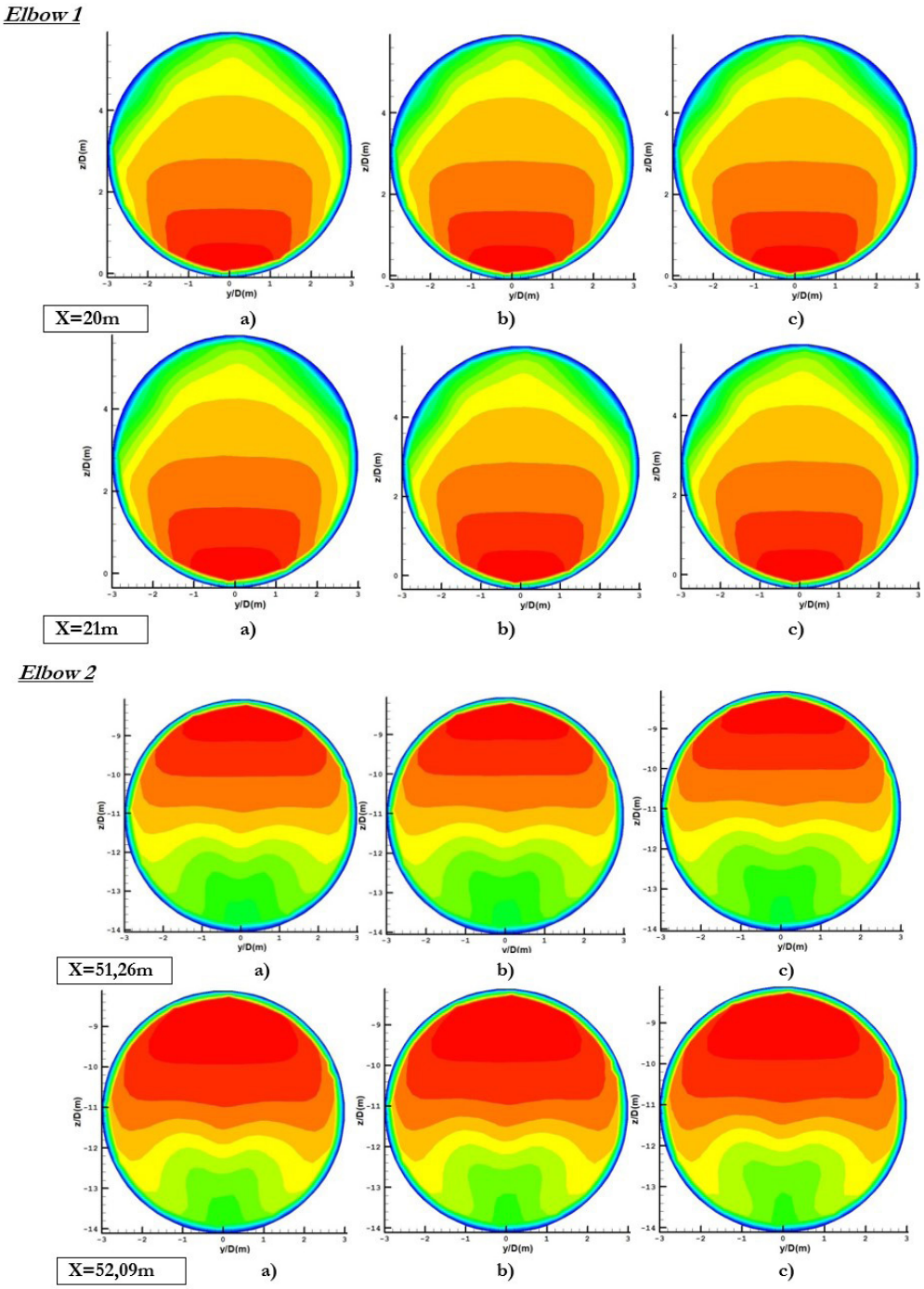

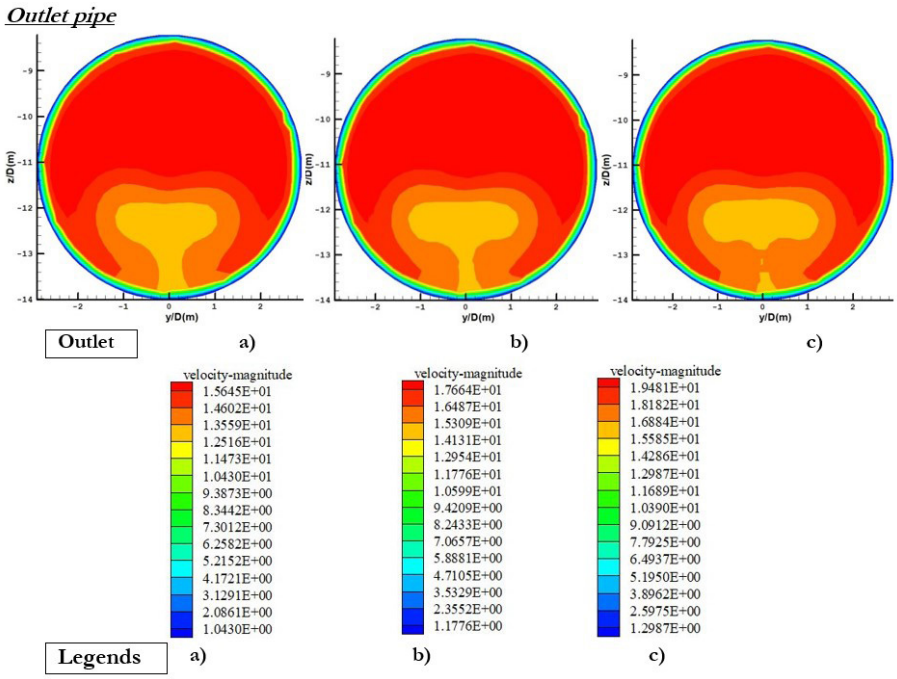

Figure 3: Velocity fields for: Re=18.6*10^6 (a), Re=21*10^6 (b) and Re=23.16*10^6 (c) in elbow 1, elbow 2 and at the outlet

At the first elbow (at X=20m and X=21m) in figure 3 above, the results of the numerical simulation do not show any physical difference in the flow structure for these three flow ranges. From the second elbow onwards, the flow structure shows the effect of the flow rate as we can see at X=51.26m and more visibly at X=52.09m with a vortex stuck on the bottom wall. This vortex is more visible and more compact with the increase of the Reynolds number at the outlet as we can see on figure 3 above. Thus, the variation of the Reynolds number participates in the excitation of the instability in the fluid layers that we have at the outlet of the penstock of this dam.

Pressure-Related Factors

This factor is the second element of the dynamic field parameter. However, in this work, we will limit ourselves to the intake flow because the pressure at the level of the curves keeps ranges of approximately identical value for each period considered. Thus, two (02) positions upstream of the water intake were adopted for the flood and low water periods. At each position, different Reynolds values were considered from the minimum to the maximum velocity. Figures 4 and 5 below show the results obtained.

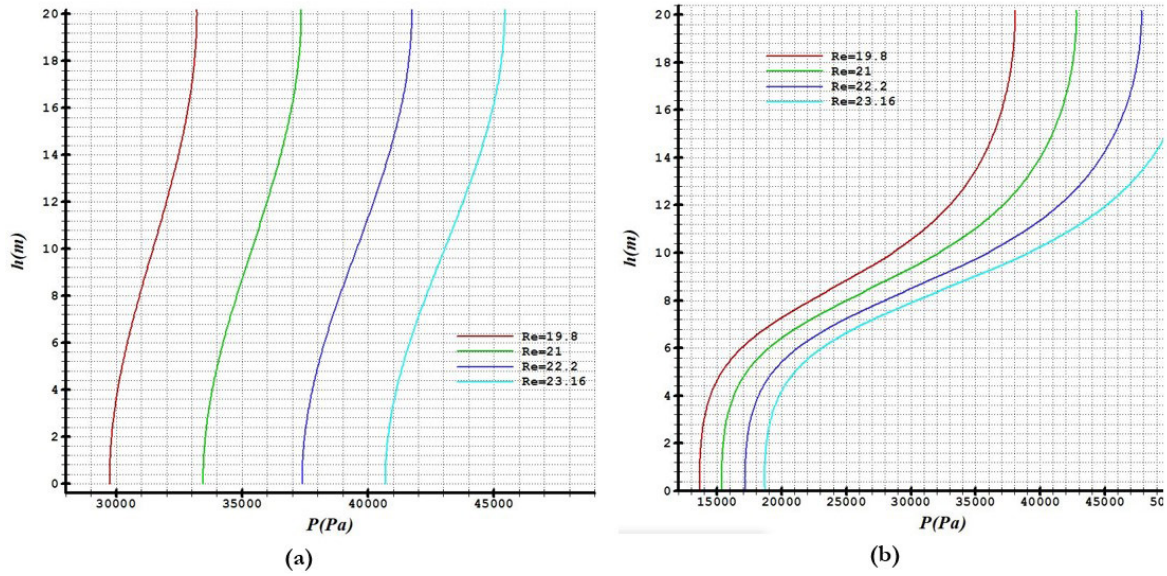

Figure 4: Pressure variation upstream of the inlet at x=-18m (a) and x=-3m (b) for different Reynolds numbers during the flood period

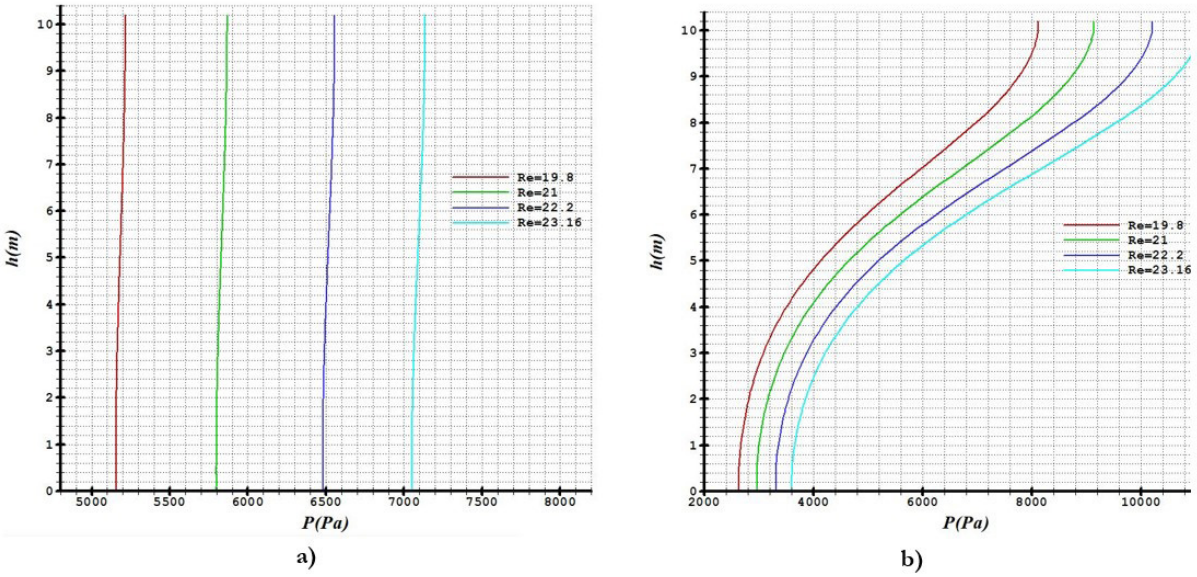

Figure 5: Pressure variation upstream of the inlet at: x=-18m (a) and x=-3m (b) for different Reynolds numbers at the low water period

It can be seen from these figures that the pressure in this area increases with the Reynolds number, and consistently for all times of the year at 18m upstream of the intake (Figure 4.a). Similarly, at 3m upstream of the intake, the pressure drops by almost 5 times near the waterbed compared to the free surface. It should also be noted that up to this distance we still do not have negative pressures (Figure 5).

Furthermore, we investigated the effect of pressure on the flow structure at six positions for the maximum flow. We observe that up to 1m upstream of the water intake, we have a non-zero pressure, whatever the period (figure 6).

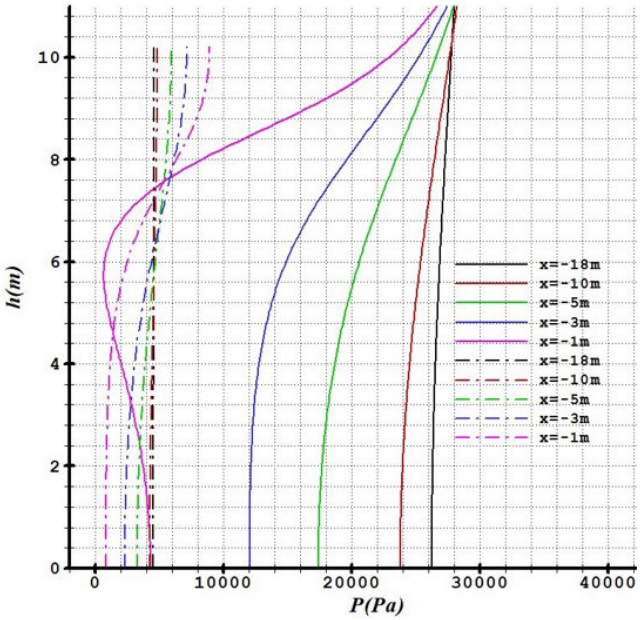

Figure 6: Pressure variation upstream of the intake at different positions of x for flood (solid lines) and low water (mixed lines) with Re= $23.16*10^6$.

We can say from this figure that the structure of the upstream flow is such that the transition zone between pressure and vacuum flows is very closely located to the water intake (less than 1m). This phenomenon creates and favours the propagation of a shock wave resulting from the sudden variation in pressure (similar to a water hammer), which propagates with severe intensity in the intake, generating instabilities in the flow structure. This is all the more important as the pressure variation for both periods is strong and summarised by: $\Delta p(e) << \Delta p(c)$ as shown in Figure 6 above. This factor relates to the one following below.

Factors Related to the Water LeveliIn the Upstream Reservoir

This factor is closely linked to the seasonal parameter because it is inseparable from flowing water within the river, and consequently from the rainfall. At 3 positions upstream of the water intake, we will show the iso-velocity and iso-pressure for each period of the year as shown in figures 7 and 8 below.

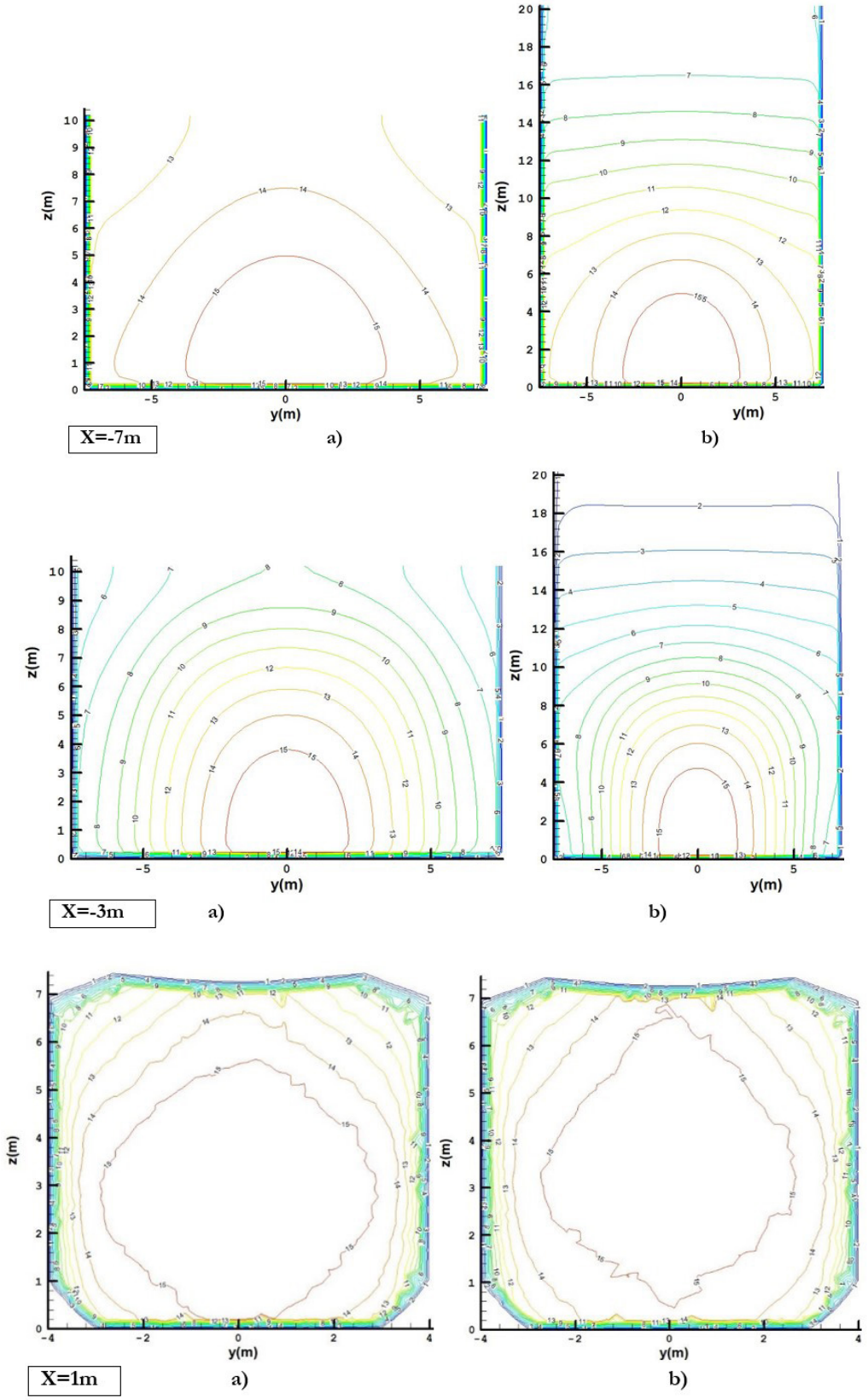

Figure 7: Iso-velocity at low water for Re=18.6*10^6 (a) and at high water for Re=23.16*10^6 (b) upstream and in the water intake

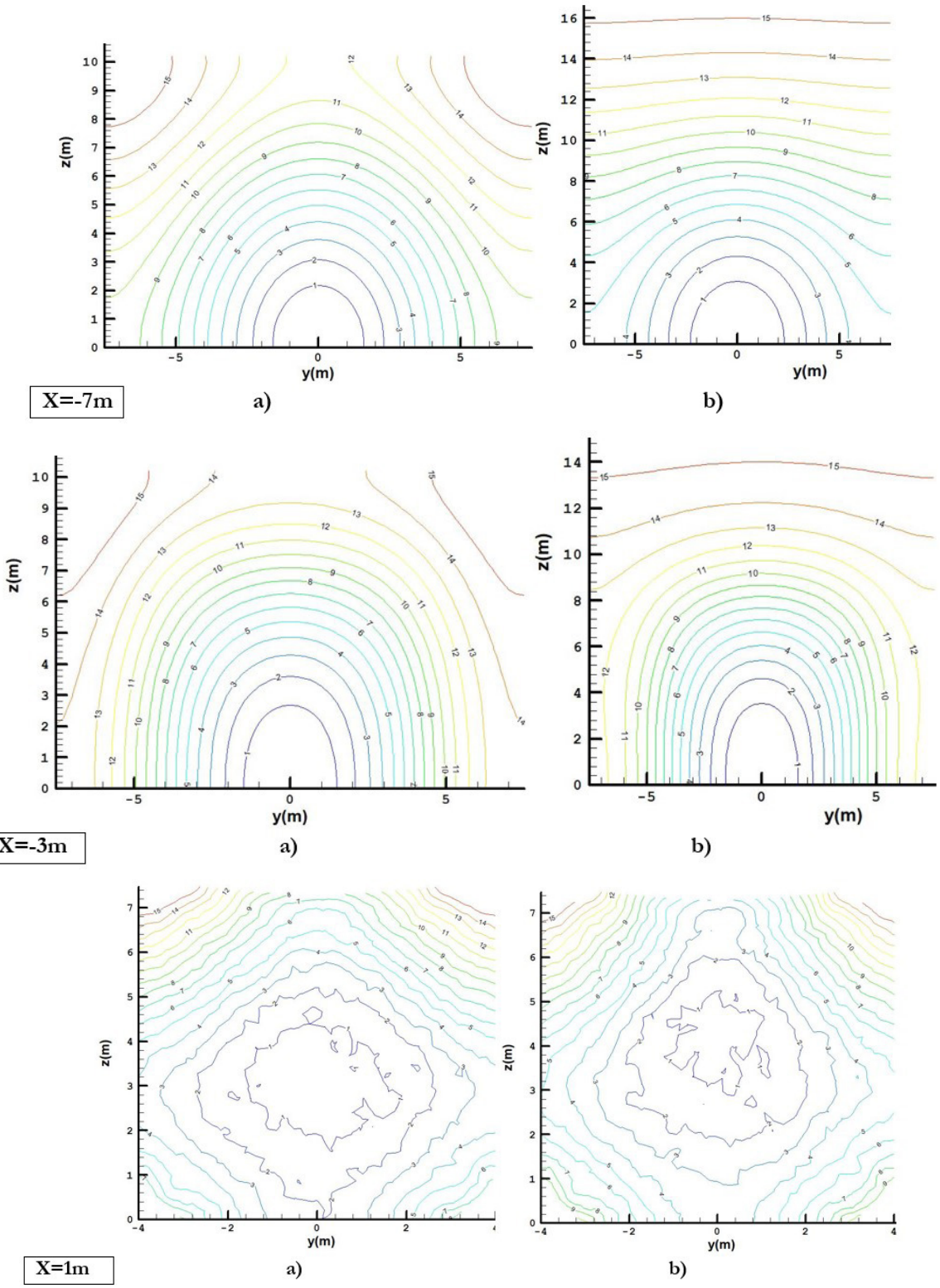

Figure 8: Iso-pressure at low water for Re=18.6*10^6 (a) and at high water for Re=23.16*10^6 (b) upstream and in the water intake

These figures show the proximity of the depression to the free surface during the low water period. This opens up the water flow in the pipe to the surface vortex at this time of year, and thus to the feeding of instabilities in the fluid layers. This aspect of the phenomenon however requires further study. In the intake, the flow structure clearly shows the unsteady character.

Another phenomenon visible on these figures is the position of the high velocity layers. These are stuck to the water bed in such a way that the amount of sediment that can be transported into the penstock is high. This then implicates another factor, which is grinding and resistance to the flow.

Friction-Related Factors

Friction in a penstock can depend on several parameters. In this section, we focus on the structural parameters of the edifice, although the other parameters mentioned above also have their impacts. After evaluating the height of the asperities influencing the boundary layer detachment, the friction coefficient is obtained graphically in each portion of the penstock. Figures 9 and 10 below illustrate the evolution of the turbulent friction on the low and high walls in the penstock for a thickness (e) of 5mm (with e = ε_{max}). These profiles are obtained for periods of low velocity in the structure.

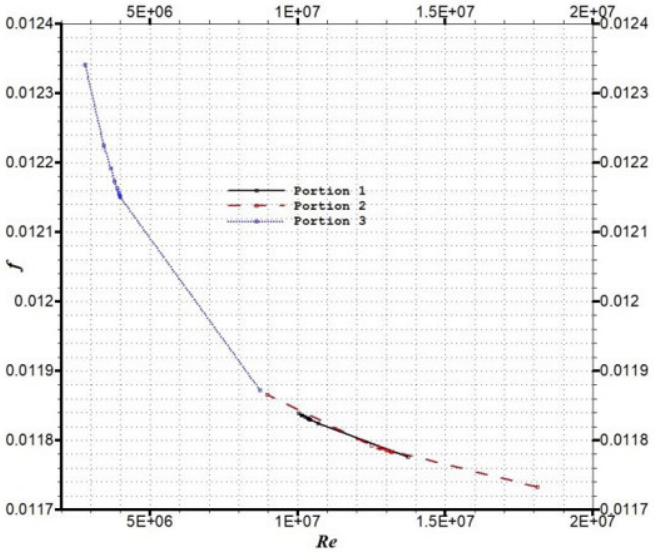

Figure 9: Evolution of the turbulent friction on the bottom wall in the three sections of the penstock

We can see that the friction coefficient is higher in the third portion of our pipe in Figure 9 above. In the same logic and with a high Reynolds number, the lowest value is observed in the second portion. The variation of the friction coefficient in the first portion can be said to be negligible compared to the other two portions.

Figure 10 below represents the evolution of the turbulent friction on the upper wall of our penstock.

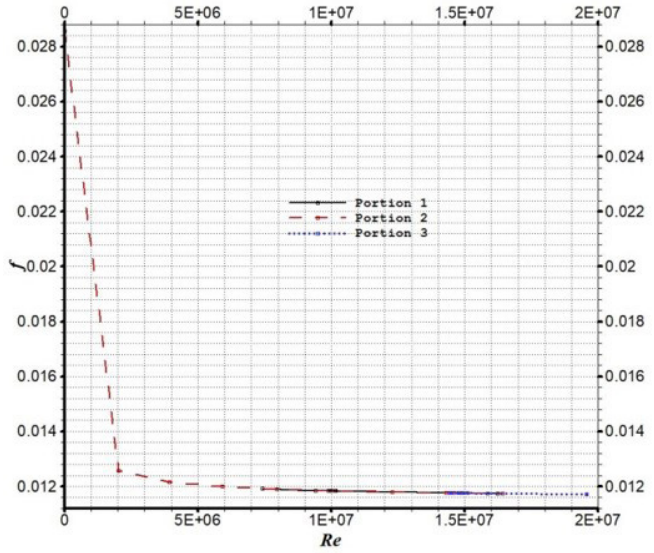

Figure 10: Evolution of the turbulent friction on the top wall in the three sections of the penstock

In this figure, the focus is on the behavior of the turbulent friction in the second section. The range of values is more pronounced and the profile is very irregular. The highest value of f is found in this section with a Reynolds number of almost zero. In contrast to this, the profiles from the other sections appear to be almost linear.

In general, in this section, we find that the value assigned to turbulent friction as determined so far by standard methods is erroneous. This is justified by the fact that f is not constant throughout the pipe. It is not the same in the same portion, nor even in the same section (whether on the bottom or the top wall). With a water intake glued to

the water bed and a sandy soil, clogging of the penstock occurs over a short period of time compared to other structures in the country. This pressing is the cause of the permanent variation of the flow structure and especially of the turbulent friction as deduced from the field. Thus, this more or less instantaneous variation would be at the origin of instabilities on the structure of the fluid in transit.

Comparative Study

Calomino & Lauria (2014) and Huang *et al.* (2015) have worked on structures with similar intake arrangements to ours. Thus, their studies helped us to validate our model. Figure 11 below shows the variation of the flow upstream of the intake for two positions.

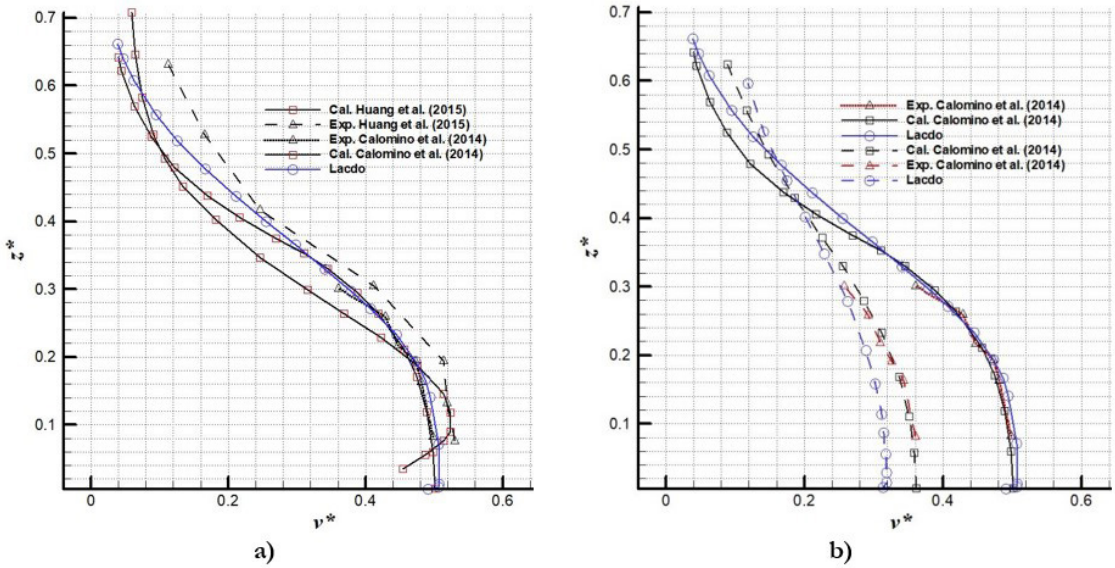

Figure 11: Evolution of the flow structure upstream of the water intake at x=-5m (a), then at x=-8m (broken lines) and at x=-5m (strong lines) (b)

The figure shows that at 5 meters from the water intake we have good agreement with the works of Calomino & Lauria (2014) (figure 11.b). At 8 meters upstream, we also have the same paces despite some discrepancies in the values. These discrepancies are mainly due to the scaling factors considered during the data acquisition. However, our results agree very favorably with this work.

In the same logic, the work of Meselhe & Odgaard (1998) present velocity vectors at the inlet of the water intake. Our vectors behave like those found within the framework of their studies, where we have the maximum speeds going towards the water bed as seen on figure 12 below.

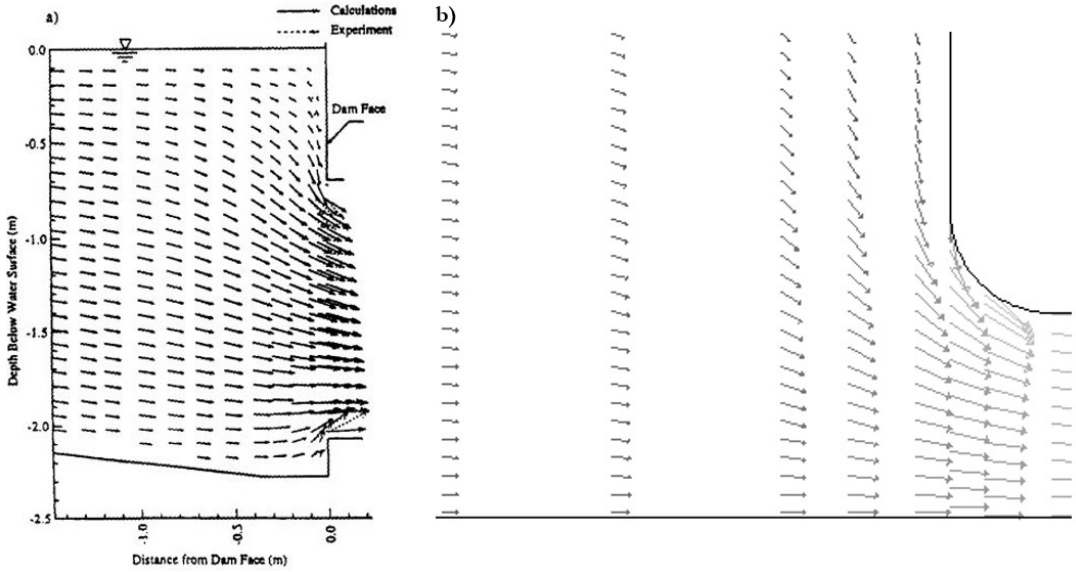

Figure 12: Velocity vectors of Meselhe & Odgaard (1998) (a), and the present study (b)

CONCLUSIONS

In this work, where the aim was to highlight the instability parameters observed at the exit of the penstock, we presented results obtained numerically after obtaining ground data. Thus, we have highlighted three main parameters at the origin of this phenomenon, namely, dynamic field parameters, seasonal parameters, and structural parameters of the edifice. These three parameters are associated with 4 factors: the velocity factor, the pressure factor, the water level factor in the reservoir and the friction factor. Regarding the velocity factor, we found that the variation of the Reynolds number participates in the excitation of the instability in the fluid layers that we have at the outlet of the penstock. This can be considered as a reality of similar structures in different countries. With regard to the pressure factor, we found that the structure of the upstream flow of this dam is such that the transition zone between pressure and vacuum flow is located very close to the water intake (less than 1m). This phenomenon creates and favours the propagation of a shock wave resulting from the sudden variation in pressure (similar to a water hammer). This propagates with severe intensity in the intake and thus generates instabilities in the flow structure. With regard to the water level factor in the structure, we observed proximity of the depression to the free surface during the low water period. This opens the water flow in the pipe to the Free surface vortex at this time of the year, and thus to the feeding of instabilities in the fluid layers. As for the friction factor, it appears that with a water intake glued to the water bed and sandy soil, the clogging of the penstock occurs over a short period of time compared to other structures in the country. This fouling is the cause of the permanent variation of the flow structure and especially of the turbulent friction as deduced from the field. Thus, this more or less instantaneous variation would be at the origin of instabilities on the structure of the fluid in transit.

Acknowledgements

We would like to thank Mr. Mbohlieu Tchawe Yossa, Ph.D student at the University of Buea who helped us improve the quality of this document.

REFERENCES

Bikidik, P. G. (2014). *Analyse du secteur de l'énergie électrique au Cameroun, Bilan des actions de plaidoyers et Système de tarification de l'électricité* (Rapport du RACE, 23 p.).

Boussinesq, J. (1897). *Théorie de l'écoulement tourbillonnant et tumultueux des liquides*. Paris.

Calomino, F., & Lauria, A. (2014). 3-D underflow of a sluice gate at a channel inlet: Experimental results and CFD simulations. *Journal of Civil Engineering and Urbanism, 4*(5), 501-508.

Energy of Cameroon (ENEO) S. A. (2017). *Global Architecture Performance Index Report – WEF.*

Huang, B., Zhu, D. Z., Shao, W., Fu, J., & Rui, J. (2015). Forebay hydraulics and fish entrainment risk assessment upstream of a high dam in China. *Journal of Hydro-environment Research, 9*, 91-103.

Meselhe, E. A., & Odgaard, A. J. (1998). 3D numerical flow model for fish diversion studies at Wanapum Dam. *Journal of Hydraulic Engineering, 124,* 1203-1214.

Ngatcha, B. N., Njitchoua, R., & Naah, E. (2002). Le barrage de Lagdo (Nord-Cameroun), Gestion intégrée des zones inondables tropicales (20 p.).

Olivier, C. (2013). Introduction à la turbulence. *Cours de l'ENSTA-ParisTech 2A*. École d'ingénieur. Introduction à la turbulence, ENSTA-ParisTech. France, 83 pp. <cel-01228137>.

Prandtl, L. (1925). Bericht über Untersuchungen zur ausgebildeten Turbulenz. *Zeitschrift für Angewandte Mathematik und Mechanik, 5*, 136.

Tchawe, T., Djiako, T., Kenmeugne, B., & Tcheukam-Toko, D. (2018). Numerical study of the flow upstream of a water intake hydroelectric dam in stationary regime. *American Journal of Energy Research, 6*(2), 35-41.

Tcheukam-Toko, D., Kongue, L., Koueni-Toko, C., Mouangue, R., & Bélorgey, M. (2012). Numerical simulation and experimental validation of boundary layer generated by a turbulent flow on a hydraulically smooth bed. Research *Journal of Applied Sciences, 7*(2), 108-112.

Tchotsoua, M. (2007). *Evaluation des risques d'inondation dans la vallée de la Bénoué en aval du barrage de Lagdo (Cameroun)* (Rapport d-expertise, 9 p.).